# Photocatalytic Reductive C-O Bond Cleavage of Alkyl Aryl Ethers by Using Carbazole Catalysts with Cesium Carbonate

Yabuta, Tatsushi

Hayashi, Masahiko

Matsubara, Ryosuke

(Citation)
Journal of Organic Chemistry,86(3):2545-2555

(Issue Date)
2021-02-05

(Resource Type)
journal article

(Version)
Accepted Manuscript

# Photocatalytic reductive C–O bond cleavage of alkyl aryl ethers by using carbazole catalysts with cesium carbonate

Tatsushi Yabuta, Masahiko Hayashi, Ryosuke Matsubara*

Department of Chemistry, Graduate School of Science, Kobe University, Nada, Kobe 657-8501, Japan

## TOC

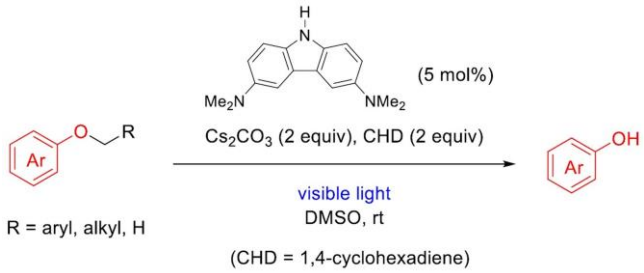


## Abstract

Methods to activate the relatively stable ether C–O bonds and convert them to other functional groups are desirable. One-electron reduction of ethers is a potentially promising route to cleave the C–O bond. However, owing to the highly negative redox potential of alkyl aryl ethers ($E^{red} < -2.6$ V vs SCE), this mode of ether C–O bond activation is challenging. Herein, we report the visible-light-induced photocatalytic cleavage of the alkyl aryl ether C–O bond using a carbazole-based organic photocatalyst. Both benzylic and non-benzylic aryl ethers underwent C–O bond cleavage to form the corresponding phenol products. Addition of $Cs_2CO_3$ was beneficial, especially in reactions using an *N*-H carbazole photocatalyst. The reaction was proposed to occur via single electron transfer (SET) from the excited-state carbazole to the substrate ether. Interaction of the *N*-H carbazole photocatalyst with $Cs_2CO_3$ via hydrogen bonding exists, which enables a deprotonation-assisted electron transfer mechanism to operate. In addition, the Lewis acidic Cs cation interacts with the substrate alkyl aryl ether to activate it as an electron acceptor. The high reducing ability of the carbazole combined with the beneficial effects of $Cs_2CO_3$ made this otherwise formidable SET event possible.

## Introduction

The alkyl aryl ether group is an abundant functional group prevalent in natural and synthesized molecules. One such important class of molecules is lignin,[1] the largest chemical

feedstock of aromatic compounds in nature. Thus, methods to activate the relatively stable C–O bonds in ethers and transform them into other functional groups are desirable. Photoredox catalysis has been extensively studied in the last decade as a powerful synthetic tool to achieve otherwise formidable bond transformations.[2] Light-induced single electron transfer (SET) can lead to C–X bond cleavage, where X is an electronegative heteroatom such as halogens, nitrogen, and oxygen, resulting in the formation of carbon radicals and X anions. However, there are very few methods to cleave the ether C–O bonds via a visible-light-induced SET mechanism. This is attributed to three main factors: (1) The large bond dissociation energy (BDE) of the ether C–O bonds (BDE = 83–86 kcal/mol),[3] (2) large negative reduction potential of ethers, and (3) weak leaving ability of alkoxides [p$K_a$ (alcohol) = 15–18].

Hasegawa[4] and Ollivier[5] reported the C–O bond cleavage of α-ketoepoxides using visible-light-active photocatalysts (Figure 1a). Helaja[6] reported the photocatalytic conversion of benzyloxypyridines to pyridones under acidic conditions (Figure 1b), in which protonation of the substrate pyridines to increase the redox potential of substrates was the key to success. Moreover, Stephenson reported the reduction of benzoyl-substituted alkyl aryl ethers using metal[7] and non-metal[8] photocatalysts (Figure 1c). However, in all these cases, the reduction potentials of the used substrates were more positive than –2.0 V vs SCE because visible-light-active photocatalysts with $E^{ox}$* [PC$^{\bullet+}$/PC*] < –2.0 V vs SCE are scarce.

Our laboratory has been focusing on the development of non-metal photocatalysts with high reducing ability.[9] We observed that the carbazole-based visible-light-activated photocatalyst **PC1**, bearing excited-state oxidation potentials as negative as –2.75 V vs SCE, exhibited high catalytic performance, enabling the reduction of unactivated chloroarenes ($E^{red}$ [PhCl/PhCl$^{\bullet-}$] = –2.88 V vs SCE) and even a fluoroarene via the SET mechanism.[10, 11, 12] The installation of dimethylamino groups at the carbazole 3- and 6-positions provided two advantages: (1) A 40 nm bathochromic shift over that of **PC2** in the absorption spectrum, enabling visible-light activation and (2) increased excited-state reducing ability [$E^{ox}$* = –2.75 V (**PC1**) vs –2.47 V (**PC2**)]. Thus, we envisioned that carbazole-based photocatalysts can be employed to attain the underdeveloped C–O bond cleavage in ethers with highly negative reduction potentials.

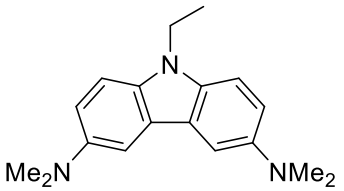

**PC1**

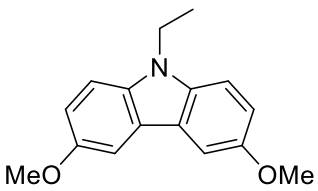

**PC2**

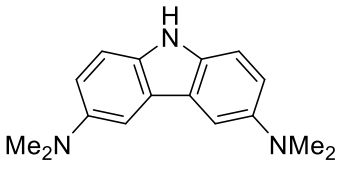

**PC3**

Herein, we report the visible-light-induced photocatalytic cleavage of alkyl aryl ether C–

O bonds ($E^{red}$ < –2.6 V vs. SCE). Notably, both benzylic and non-benzylic aryl ethers underwent C–O bond cleavage (Figure 1d). Moreover, the catalytic performance of the *N*-H-type carbazole **PC3** was superior to that of **PC1**, which is experimentally rationalized.

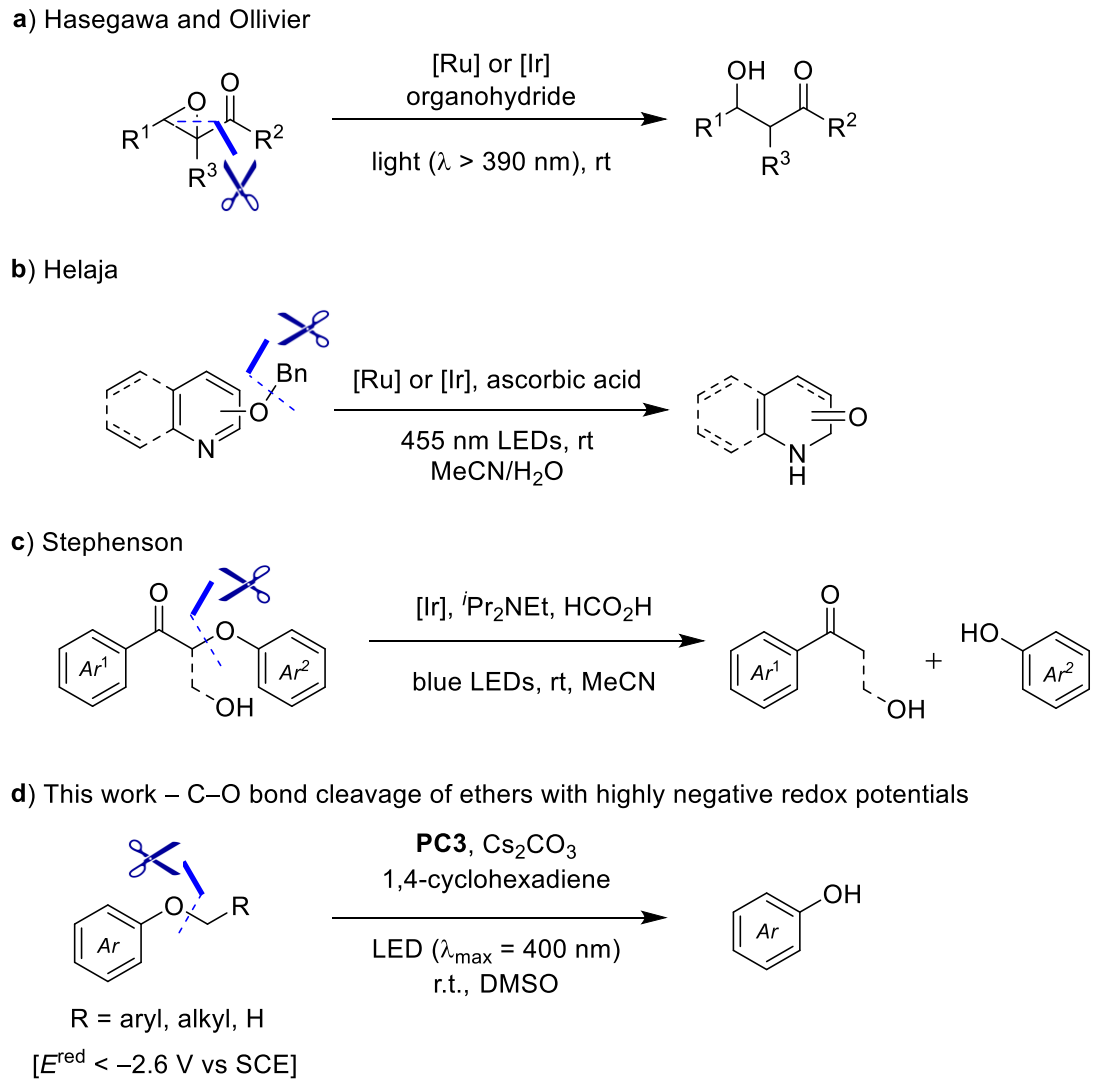


**Figure 1.** Visible-light-induced photocatalytic C–O bond cleavage of ethers.

## Results and discussion

Benzyl phenyl ether (**1a**) did not display any reduction wave within the potential window of the acetonitrile solvent (Figure S1), indicating that **1a** has a reduction potential $E^{red}$ < –2.6 V vs SCE. Indeed, this is a class of molecules that cannot be reduced by commonly used photocatalysts such as $Ru(bpy)_3Cl_2$ and $Ir(ppy)_3$. We therefore began our investigations by using **1a** as the model substrate and carbazole-based photocatalysts (Table 1). Thus, we first tested previously developed conditions for the dechlorination of aryl chlorides, namely **PC1**

(5 mol%), $^{i}Pr_2NEt$ (2 equiv), and 1,4-cyclohexadiene (CHD; 2 equiv) in *N*,*N*-dimethylacetamide (DMA).[10] After 24 h of irradiation using an LED lamp (λ = 400 ± 20 nm), phenol (**2a**) was obtained in 11% yield and unreacted **1a** was recovered (entry 1). Next, we replaced **PC1** with the *N*-H variant **PC3**, the synthesis of which was previously developed by our group.[13] This led to a 23% increase in the yield of **2a** (entry 2)and therefore, we conducted the subsequent investigations with **PC3**. Rapid screening of the base and solvent revealed that $Cs_2CO_3$ and DMSO were the best base and solvent, respectively (entries 3–8). Addition of $Bu_4NBr$ to increase the solubility of base did not improve the yield (entry 9). Notably, in the absence of CHD, the reaction proceeded with a slightly decreased yield (entry 10). We next changed the catalyst loading (entries 11 and 12); however, no significant difference in product yield was observed. This result can be interpreted as follows: under this condition, even as low as 2.5 mol% of **PC3** was enough to absorb most of the supplied photons; so the increase of the photocatalyst amount did not lead to the acceleration of the reaction. In the absence of a photocatalyst, the reaction proceeded to afford **2a** in 10% yield (entry 13). This result was unexpected given that on their own, none of the species displayed absorption in the wavelength region of the employed light source, as discussed later. The amount of $Cs_2CO_3$ affected the reaction rate (entries 14–17), so that the yield decreased with decreasing amount of $Cs_2CO_3$. This $Cs_2CO_3$ effect was also observed in the photocatalysis reactions using **PC1** (entries 18 and 19). These results provided insight into the reaction mechanism and are discussed later. As predicted, no reaction occurred in the dark (entry 20).

**Table 1.** Optimization of the photochemical C–O bond cleavage of **1a**[a]

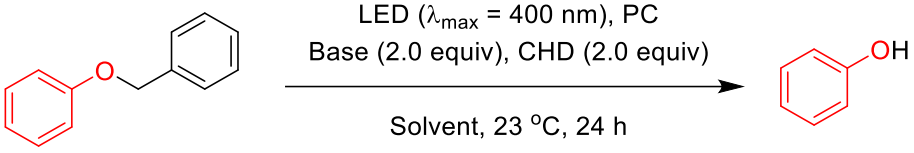


**1a** **2a**

| Entry | PC (mol%) | Base | Solvent | Yield /%[b] **2a** | **1a** |
|---|---|---|---|---|---|
| 1 | **PC1** (5) | *i*-$Pr_2NEt$ | DMA | 11[c] | 80[c] |
| 2 | **PC3** (5) | *i*-$Pr_2NEt$ | DMA | 23[c] | 78[c] |
| 3 | **PC3** (5) | $Cs_2CO_3$ | DMA | 34 | 65 |
| 4 | **PC3** (5) | $K_2CO_3$ | DMA | 20 | 76 |
| 5 | **PC3** (5) | $K_3PO_4$ | DMA | 31 | 61 |
| 6 | **PC3** (5) | $Cs_2CO_3$ | $CH_3CN$ | 21 | 78 |

| | | | | | |
|---|---|---|---|---|---|
| 7 | **PC3** (5) | $Cs_2CO_3$ | DMF | 22 | 69 |
| 8 | **PC3** (5) | $Cs_2CO_3$ | DMSO | 48 | 50 |
| 9[d] | **PC3** (5) | $Cs_2CO_3$ | DMSO | 43 | 53 |
| 10[e] | **PC3** (5) | $Cs_2CO_3$ | DMSO | 40 | 53 |
| 11 | **PC3** (8) | $Cs_2CO_3$ | DMSO | 49 | 46 |
| 12 | **PC3** (2.5) | $Cs_2CO_3$ | DMSO | 46 | 48 |
| 13 | – | $Cs_2CO_3$ | DMSO | 10 | 91 |
| 14[f] | **PC3** (5) | $Cs_2CO_3$ | DMSO | 63 | 32 |
| 15[f] | **PC3** (5) | $Cs_2CO_3$ (1.0 equiv) | DMSO | 55 | 40 |
| 16[f] | **PC3** (5) | $Cs_2CO_3$ (0.5 equiv) | DMSO | 37 | 60 |
| 17[f] | **PC3** (5) | – | DMSO | 17 | 80 |
| 18[f] | **PC1** (5) | $Cs_2CO_3$ | DMSO | 52 | 37 |
| 19[f] | **PC1** (5) | – | DMSO | 27 | 65 |
| 20[g] | **PC3** (5) | $Cs_2CO_3$ | DMSO | 0 | quant |

[a] Conditions: **1a** (0.5 mmol, 1.0 equiv), PC, base (2.0 equiv), CHD (2.0 equiv), solvent (5.0 mL, 0.1 M), LED ($\lambda_{max}$ = 400 nm), argon atmosphere, 23 °C, Pyrex tube. [b] Determined by reverse-phase HPLC. [c] Determined by $^1$H NMR analysis using 1,3,5-trimethoxybenzene as the internal standard. [d] With $Bu_4NBr$ (1 equiv). [e] Without CHD. [f] 48 h. [g] No light. Abbreviations: PC = photocatalyst, CHD = 1,4-cyclohexadiene, DMA = *N,N*-dimethylacetamide, DMF = dimethylformamide, and DMSO = dimethylsulfoxide.

With the optimized reaction conditions in hand (see entry 14 of Table 1), the scope of the developed ether C–O bond cleavage was next examined (Table 2). The reactions proceeded smoothly with aryl benzyl ethers bearing electron-withdrawing substituents (entries 1–6). The reaction on a 2-mmol scale uneventfully proceeded (entry 1). The reaction was sluggish with aryl benzyl ether **1h** bearing an electron-donating substituent (entry 7). Both the regioisomers of naphthyl benzyl ethers **1i** and **1j** were good substrates (entries 8 and 9). Because polyaryl phenolates were recently reported to have photocatalytic activities,[14] we checked the photocatalytic activity of the phenol product. The C–O bond cleavage of **1j** was conducted under the same reaction condition as entry 9 of Table 2 except using 5 mol% of 1-naphthol (**2i**) as a photocatalyst instead of **PC3**. After 15 hours, product **2j** was obtained in 64% yield, a comparable result with that of the reaction using **PC3** (entry 9, Table 2). This suggests that in some instances product phenolates may potentially self-catalyze the reaction. Aryl *p*-methoxybenzyl (PMB) ethers were also examined (entries 10–14) as both benzyl and

PMB ethers are commonly utilized as a protecting group for hydroxyl groups in the target-oriented synthesis. These reactions took longer than those of the corresponding benzyl ethers, probably because the electron-donating *p*-MeO group slowed the SET event from the excited-state **PC3** to the substrates; nevertheless, the expected products were obtained in acceptable yields. Alkyl benzyl ether **1p** was also tested (entry 15) and although the reaction was slow, product alcohol **2k** was obtained in 15% yield. Next, alkyl aryl ethers **1q–s** were subjected to the proposed reaction system (entries 16–18) wherein surprisingly, product **2b** was generated in high yields. Thus, it became apparent that the developed reaction conditions can be applicable to both benzyl- and non-benzyl-type ethers. The quantum yield of photochemical C–O bond cleavage of **1b** was determined to be 0.16.

**Table 2.** Substrate scope[a]

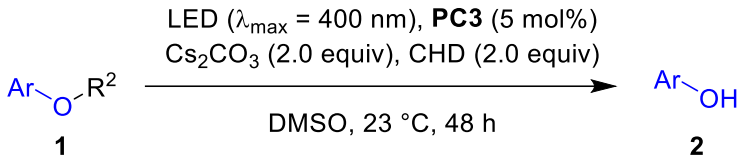


**1** **2**

| Entry | Substrate | Product | Yield /% (Time)[b] | Entry | Substrate | Product | Yield /% (Time)[b] |
|---|---|---|---|---|---|---|---|
| 1 | 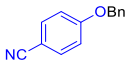 **1b** | 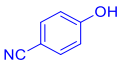 **2b** | 99 (18 h) 98[c] (29 h) | 10 | 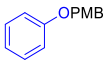 **1k** |  **2a** | 51[f] |
| 2 | 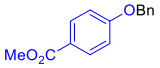 **1c** | 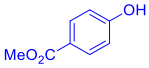 **2c** | >99 (44 h) | 11 | 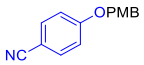 **1l** | 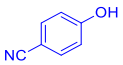 **2b** | 93 (36 h) |
| 3 | 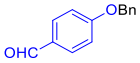 **1d** | 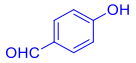 **2d** | 69[d] | 12 | 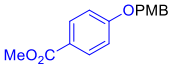 **1m** | 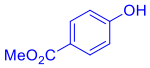 **2c** | 78 |
| 4 | 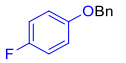 **1e** | 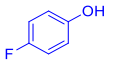 **2e** | 68[e] | 13 | 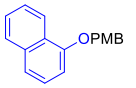 **1n** | 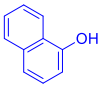 **2i** | 48 (6 h) |
| 5 | 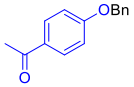 **1f** | 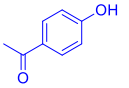 **2f** | 43 | 14 | 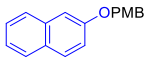 **1o** | 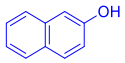 **2j** | 43 |
| 6 | 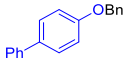 **1g** | 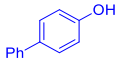 **2g** | 70 | 15 |  **1p** |  **2k** | 15[d] |
| 7 | 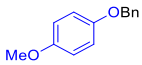 **1h** | 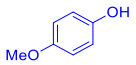 **2h** | 40 | 16 | 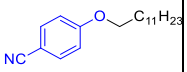 **1q** | 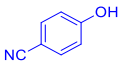 **2b** | >99[d] |
| 8 | 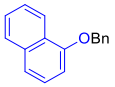 **1i** | 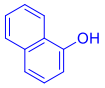 **2i** | 55[d] (3 h) | 17 | 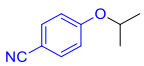 **1r** | 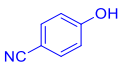 **2b** | 90 (22 h) |
| 9 | 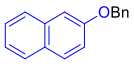 **1j** | 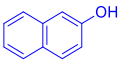 **2j** | 62 (24 h) | 18 | 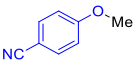 **1s** | 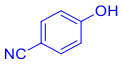 **2b** | 94 |

[a] Conditions: Substrate (0.5 mmol, 1.0 equiv), **PC3** (5 mol%), $Cs_2CO_3$ (2.0 equiv), CHD (2.0 equiv), DMSO (5.0 mL, 0.1 M), LED ($\lambda_{max}$ = 400 nm), argon atmosphere, 23 °C, 48 h, Pyrex tube; isolated yield shown unless otherwise noted. [b] Reaction time shown unless it was 48 h. [c] 2 mmol scale. [d] Determined by $^1$H NMR analysis using 1,3,5-trimethoxybenzene as the internal standard. [e] Determined by $^{19}$F NMR analysis using fluorobenzene as the internal standard. [f] Determined by RP-HPLC analysis. Abbreviation: PMB = *p*-methoxybenzyl.

## Mechanistic study

A detailed mechanistic study was next conducted to clarify the pronounced role of $Cs_2CO_3$, which markedly accelerated the photochemical reactions (Table 1, entries 14–19).

The electronic and optical properties of **PC3** were first studied, and the results are compared to those of **PC1** in Figure 2.[10] Cyclic voltammetric analysis revealed that based on the first reversible oxidation event, the redox potential of **PC3**, $E^{ox}$ [**PC3**$^{\bullet+}$/**PC3**], was +0.29 V vs SCE (Figure 2a). This value is similar to that of **PC1** ($E^{ox}$ [**PC1**$^{\bullet+}$/**PC1**] = +0.27 V vs SCE). The absorption and fluorescence spectra of **PC1** and **PC3** did not display any significant differences (Figure 2b and 2c, respectively). The lowest energy peak of **PC3** in the absorption spectrum is attributed to the HOMO → LUMO transition. Because the HOMO energy level increases, owing to the electron-donating $NMe_2$ groups at the 3- and 6-positions, the HOMO-LUMO gap becomes smaller resulting in a longer absorption wavelength that reaches the visible region. From the onset value of the fluorescence emission peak (407 nm), the excited state of **PC3** was estimated to be 3.05 eV above the ground state. Thus, from the Rehm-Weller equation,[15] the excited-state oxidation potential of **PC3** is $E^{ox}$* [**PC3**$^{\bullet+}$/**PC3***] = +0.29 – 3.05 = –2.76 V vs SCE. This value is similar to that of **PC1** (–2.75 V vs SCE).[10]

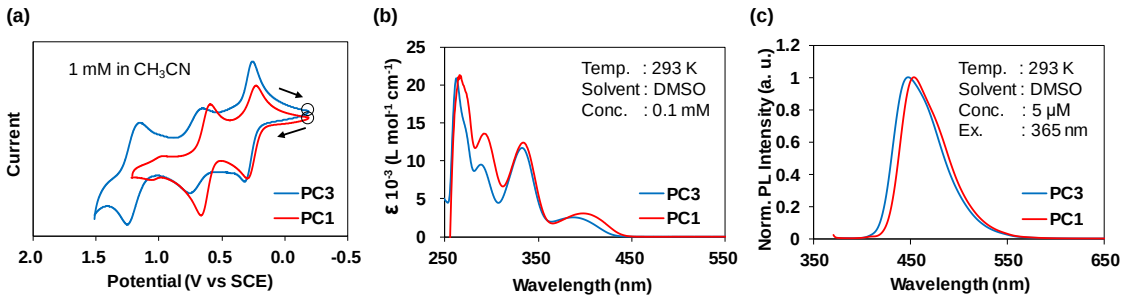


**Figure 2.** Electronic and optical properties of **PC3**. Those of **PC1** are also shown for comparison.[10] (a) Cyclic voltammetric (the black circles indicate the potentials from which the scans originated), (b) UV-vis absorption, and (c) fluorescence spectra.

The addition of $Cs_2CO_3$ significantly increased the reaction rate of the photochemical C–O bond cleavage of ethers. This positive effect of $Cs_2CO_3$ was observed both in the reactions using **PC3** (from 17% to 63% yield; Table 1, entries 14 and 17) and **PC1** (from 27% to 52% yield; Table 1, entries 18 and 19). Larionov recently reported that an *N*-H type phenothiazine photocatalyst interacts with a carbonate anion and enhances its reducing ability.[16] This led us to suppose that a similar activation process operates in the reactions using **PC3**. We therefore measured the absorption and fluorescence spectra of **PC1** and **PC3** in the presence of $Cs_2CO_3$ and compared them to those attained in the absence of $Cs_2CO_3$ to establish whether there were any significant changes between the two sets of spectra. The inorganic salt $Cs_2CO_3$ was barely soluble in DMSO and remained insoluble in the photochemical reactions in this study. Thus, to reproduce the conditions of the actual photochemical reaction in the spectroscopic measurements, the analytical samples were prepared by saturating the photocatalyst solution with $Cs_2CO_3$. The spectroscopic measurements were conducted 5 min after shaking, when all the insoluble solid settled at the bottom of the measurement cuvettes. In the absorption spectrum of **PC3** in the presence of $Cs_2CO_3$, new peaks appeared at 440 nm and 300 nm (Figure 3a), suggesting that a new species between **PC3** and $Cs_2CO_3$ was generated. No such change was observed for **PC1** (Figure 3b), which implies that the **PC3** N–H proton interacts with $Cs_2CO_3$, probably via hydrogen bonding, as suggested by Larionov[16]This notion does not contradict the $^1$H NMR spectroscopic results wherein, upon the addition of $Cs_2CO_3$, the N–H peak (marked with the symbol "*" in the chart) disappeared and an upfield shift of the aromatic protons was observed (Figure 3c).[17] This change was more prominent in the fluorescence spectra (Figure 3d). The sample at 5 min after shaking displayed new red-shifted peaks ($\lambda_{max}$ at 505 nm) in addition to the original **PC3** peaks ($\lambda_{max}$ at 447 nm). With the elapse of time, from 5 to 55 min, the new peaks decreased, and the original peaks increased with a clear isofluorescent point at 490 nm. The fluorescence spectrum at 55 min was almost identical to that observed in the absence of $Cs_2CO_3$ (Figure 2c). This sample was remixed well by shaking and then reanalyzed. The red-shifted peaks with $\lambda_{max}$ at 505 nm reappeared (Figure 3e), indicating that the structural change was reversible. For the DMSO solution of **PC3** with $Cs_2CO_3$ at 5 min after preparation (red fluorescence spectrum in Figure 3d), the excitation spectra were measured by monitoring varied wavelengths of fluorescence (Figure 3f). The observed excitation spectra attained from fluorescence emission at 450 and 560 nm are almost superimposable to the absorption spectra of **PC3** without and with $Cs_2CO_3$, respectively (Figure 3a). This further supported that upon mixing with $Cs_2CO_3$, **PC3** provided a spectroscopically distinct complex. The cyclic voltammogram of **PC3** in the presence of $Cs_2CO_3$ was similar to that in its absence (Figure S5). Overall, the above observations as well as the literature precedent[16] do not contradict the notion that **PC3** interacts with $Cs_2CO_3$ via

a hydrogen bonding to give the weakly-bound complex. However, the possibility that the neutral and deprotonated forms of **PC3** are in equilibrium cannot be ruled out (see Supporting Information for a more detailed discussion).

Fluorescence quenching experiments of **PC3** with substrate **1a** and CHD were next performed (Figure 3g). Fluorescence quenching was observed with **1a** both in the presence and absence of $Cs_2CO_3$, with significantly stronger quenching observed in the former. It is of note that in this study the fluorescence intensity at 447 nm was plotted because, in the presence of **PC3**, the red-shifted peaks with $\lambda_{max}$ at 505 nm, which is attributed to the complex generated from **PC3** and $Cs_2CO_3$, was very weak. The reason for this observation is unclear at present. On the other hand, CHD did not result in fluorescence quenching of **PC3**, regardless of the presence of $Cs_2CO_3$. These results do not contradict the notion that **PC3** functions as a photocatalyst via the oxidative quenching pathway rather than the reductive quenching pathway, although the other reaction pathways cannot be completely ruled out. Although in the presence of ether substrate **1a** the complex generated from **PC3** and $Cs_2CO_3$ could not be detected spectroscopically, we speculate that in the actual photochemical reactions a stirring helps the formation of this complex and that this complex bears greater reducing ability than **PC3** itself.

The above conclusion cannot rationalize the experimental results wherein the addition of $Cs_2CO_3$ also accelerated photocatalytic reaction in the presence of **PC1** (Table 1, entries 18 vs 19), given that **PC1** does not have an N–H proton that can interact with $Cs_2CO_3$. We therefore proceeded to examine the interaction of $Cs_2CO_3$ with a substrate ether by absorption spectroscopy. Upon addition of $Cs_2CO_3$ to the solution of **1a**, a new absorption peak with $\lambda_{max}$ at 320 nm appeared (Figure 3h), indicating a weak but non-negligible interaction between $Cs_2CO_3$ and **1a**. Because **1a** does not contain any acidic protons, we assumed that a Lewis acidic Cs cation coordinates to the ether oxygen lone pair to enhance the electron accepting ability of **1a** (see Supporting Information for a more detailed discussion).[18] This assumption does not contradict the fact that the switch from Cs to a weaker Lewis acid potassium counter cation caused a drop in yield (Table 1, entries 3 vs 4). Additionally, owing to this bathochromic shift of **1a** absorption caused by $Cs_2CO_3$, the emission spectrum of the employed LED lamp overlaps, albeit marginally, with the absorption spectrum of **1a** (Figure S2). It is surmised that this overlap results in the photochemical C–O bond cleavage (10% yield) of **1a** in the absence of a photocatalyst, probably via homolytic bond scission (Table 1, entry 13).[19]

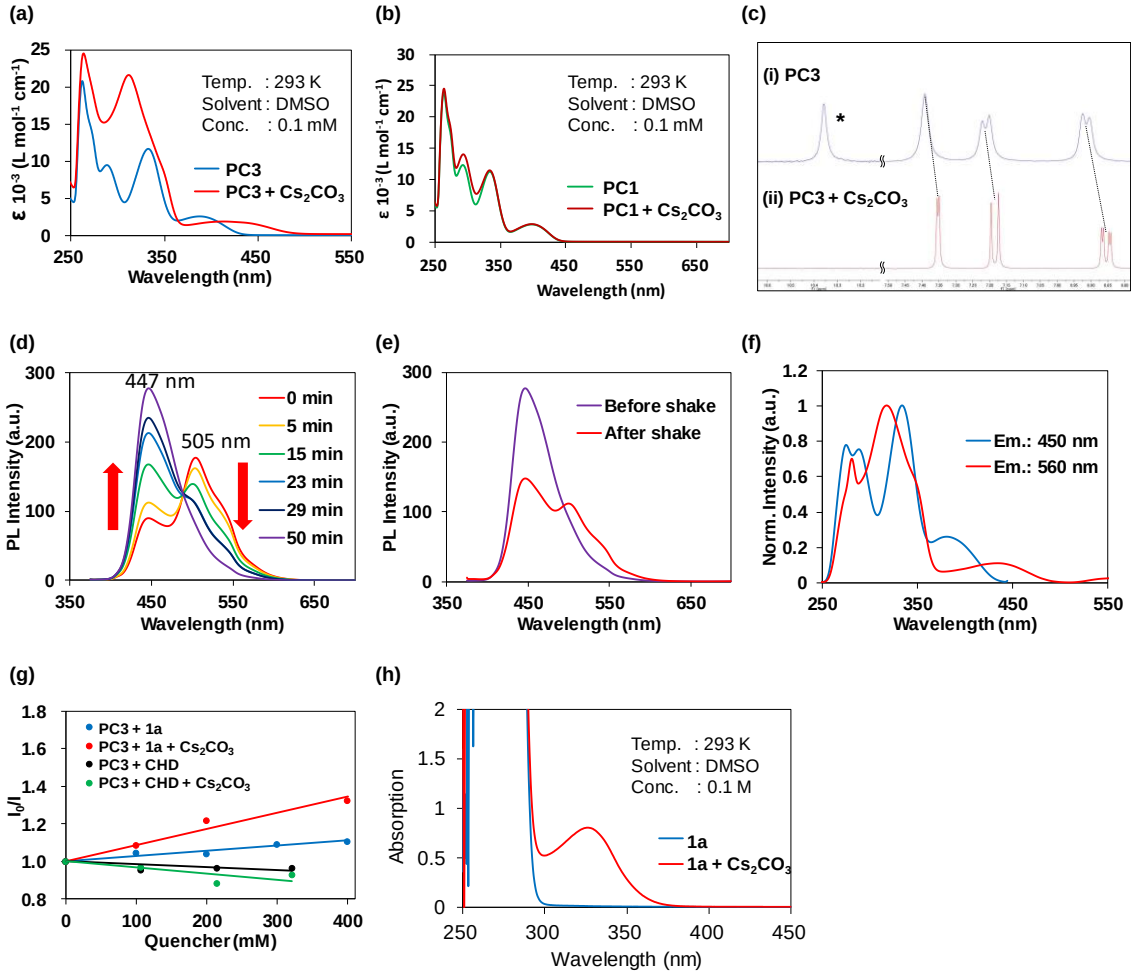


**Figure 3.** Study of the effects of $Cs_2CO_3$. (a,b) Changes in the UV-vis absorption of **PC3** and **PC1**. (c) Changes in the $^1H$ NMR spectra of **PC3**; solvent: DMSO. (d) Changes in the fluorescence spectra of **PC3**. The measurements were conducted after the intervals indicated in the legend after the addition of $Cs_2CO_3$; solvent: DMSO. (e) **PC3** solution 55 min after the addition of $Cs_2CO_3$ (corresponding to the purple spectrum in Figure 3d), which was mixed by shaking. Changes in the fluorescence spectra were observed before (purple) and after (red) shaking; solvent: DMSO. (f) Excitation spectra of **PC3** in the presence of $Cs_2CO_3$ attained by observing fluorescence at 450 and 560 nm; solvent: DMSO. (g) Fluorescence quenching experiment of **PC3** with quencher candidates (**1a** or CHD); solvent: DMSO, Ex: 365 nm. (h) Changes in the UV-vis absorption of **1a**. See Experimental section for more detail.

**Scheme 1.** Analysis of the co-products

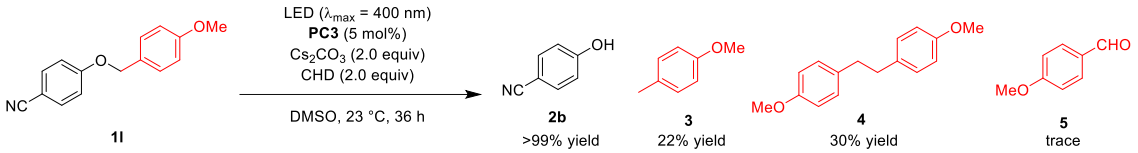


To determine the outcome of the cleaved benzyl counterpart, quantitative analysis of the co-products generated along with the phenol products was carried out for the photochemical reaction of **1l** (Scheme 1). *p*-Methoxytoluene (**3**) and 4,4'-dimethoxybibenzyl (**4**) were observed in 22% and 30% yields, respectively. The formation of **4** is firm evidence of the formation of a benzylic radical. Anisaldehyde (**5**) was also generated, albeit in trace amounts, probably via oxidation of the benzyl radical to the benzyl cation followed by DMSO oxidation.

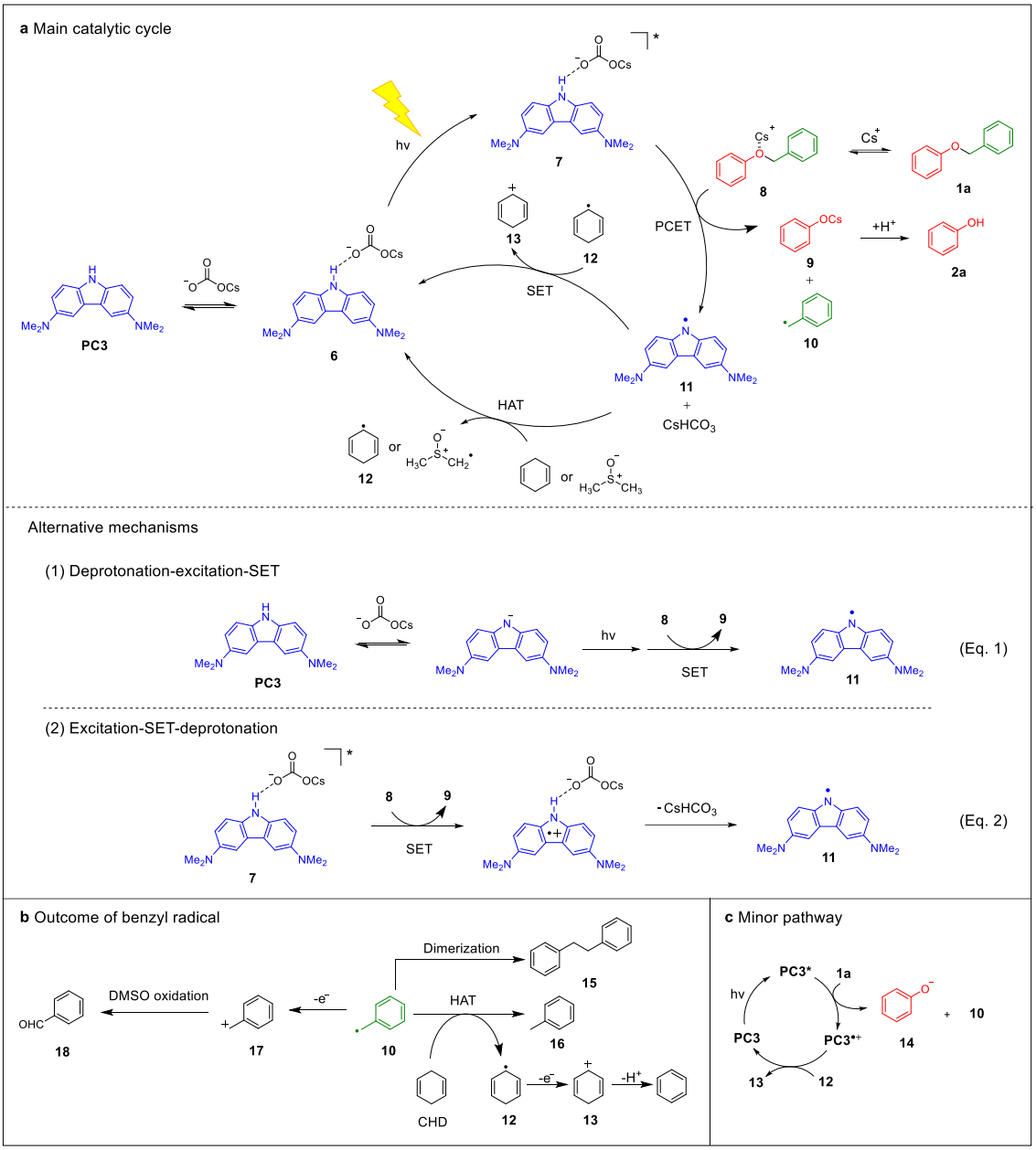


**Figure 4.** Proposed reaction mechanism

Based on the above experimental results, a catalytic mechanism for the C–O bond cleavage of ethers using **PC3** is proposed (Figure 4a with substrate **1a** as a representative example) as follows: The **PC3** N–H proton interacts via hydrogen bonding with a carbonate anion to form complex **6**. Photoirradiation of **6** generates excited state **7**, which exhibits a high reducing ability. Substrate ether **1a** coordinates with the Lewis acidic Cs cation to form complex **8**, which is a better electron acceptor than **1a**. Subsequent electron transfer from **7** to **8** affords phenoxide **9** and benzyl radical **10**. This process involves a proton-coupled electron transfer

(PCET) mechanism[20] that diminishes the required energy barrier. The resulting neutral radical **11** is a strong hydrogen atom acceptor, which undergoes hydrogen atom transfer (HAT) with CHD or DMSO solvent, thereby regenerating **6**. As alternatives to the PCET mechanism, the pathways in which deprotonation and SET occur stepwise are possible (Eq. 1 and 2). Benzyl radical **10** is mainly converted to **15** via dimerization or to toluene (**16**) via HAT with CHD (Figure 4b). Part of **10** is converted to benzaldehyde **18** via benzyl cation **17**. Throughout the process, CHD serves as a good hydrogen atom donor with its low BDE (76.0 kcal $mol^{-1}$) as the driving force.[21] Radical species **12**, which is generated from CHD after the HAT event, operates as a good electron donor. The photochemical reaction proceeded even in the absence of CHD, however, in lower yield (Table 1, entry 10). We speculated that in this case, DMSO (BDE = 94 kcal $mol^{-1}$)[22] serves as a hydrogen atom donor to react with **11** [BDE (carbazole N–H) = 92.7 kcal $mol^{-1}$].[23] Given that the C–O bond cleavage of **1a** occurred, although sluggishly, even in the absence of $Cs_2CO_3$ (Table 1, entry 17), we supposed that a simple photoredox cycle without the involvement of $Cs_2CO_3$ should also exist as a minor pathway (Figure 4c).

## Conclusion

In conclusion, we have developed a photocatalytic reductive cleavage of the C–O bond in alkyl aryl ethers using a visible-light-active carbazole derivative as an organic photocatalyst. The ether C–O bonds of both benzylic and non-benzylic aryl ethers were cleaved to afford phenol derivatives in good yields. The reaction was proposed to occur via SET from the excited-state carbazole to the substrate ether. The superior activity of the *N*-H carbazole photocatalyst over that of the *N*-alkyl variant, in the presence of a base, together with supporting spectroscopic data suggested a deprotonation-assisted electron transfer mechanism to achieve this otherwise formidable SET event.

## Experimental Section

***General*** All reactions were carried out in well-cleaned and oven-dried glassware with magnetic stirring. Operations were performed under an atmosphere of dry argon using Schlenk and vacuum techniques. The heated reactions were conducted using oil baths and the oil bath temperatures are indicated. The photochemical reactions were conducted using self-manufactured LED lamp sets (see the Supporting Information for details). $^{1}H$ and $^{13}C\{^{1}H\}$ NMR spectra (400 and 100 MHz, respectively) were recorded on a Bruker Avance III HD 400 using TMS (0 ppm) and $CDCl_3$ (77.0 ppm) in $CDCl_3$ and residual MeOH (3.31 ppm) and $CD_3OD$ (49.00 ppm) in $CD_3OD$ as internal standards, respectively. The following abbreviations are used in connection with NMR: d = doublet, t = triplet, and m = multiplet.

Preparative column chromatography was performed using Kanto Chemical silica gel 60 N (spherical, neutral). Thin layer chromatography (TLC) was carried out on Merck 25 TLC silica gel 60 $F_{254}$ aluminum sheets. All starting materials were obtained from commercial sources unless otherwise noted. Photoluminescence spectra were recorded on a spectrofluorometer (Jasco FP-6500) with a quartz absorption cuvette (light path: 1 cm). UV-vis spectra were recorded on a Jasco V-670 spectrophotometer with a quartz absorption cuvette (light path: 1 cm). Cyclic voltammetric measurements were performed at 298 K on an ALS CHI606S electrochemical analyzer, using a solvent deaerated by Ar bubbling for 30 min before each measurement. The supporting electrolyte was 0.10 M $TBAClO_4$. A conventional three-electrode cell with a platinum working electrode and platinum wire as the counter electrode was employed. The cyclic voltammograms were recorded with respect to the $Ag/AgNO_3$ (10 mM) reference electrode at a sweep rate of 50 mV/s. The reduction or oxidation potentials (determined as the peak potentials) were corrected to the SCE scale based on the measurement of the $Fc/Fc^+$ couple redox potential as the standard (0.43 V vs SCE).[24] RP-HPLC analyses were performed using a Hitachi High-Tech LaChrome Elite high-performance liquid chromatograph equipped with a Mightysil RP-18 GP Aqua 150 × 4.6 mm (5 μm) column. The calibration curve was constructed using anisole as the internal standard.

***Synthesis of PC3***[13] $Pd_2(dba)_3$ (28.2 mg, 0.031 mmol, 1 mol%), RuPhos (34.5 mg, 0.074 mmol, 2.4 mol%), and THF (3 mL) were added into a Schlenk tube. The mixture was stirred at 80 °C for 15 min. After cooling, a solution of 3,6-dibromocarbazole (1.0 g, 3.08 mmol, 1.0 equiv) in THF (6 mL) was added, followed by dimethylamine hydrochloride (0.75 g, 9.2 mmol, 3.0 equiv), LiHMDS (3.60 g, 21.5 mmol, 7.0 equiv), and THF (6.4 mL). The mixture was stirred at 90 °C for 8 h. After the reaction was completed, 40 mL of 1 M HCl aq. was added to quench the reaction. The resultant mixture was washed five times with dichloromethane. Next, sat. $NaHCO_3$ aq. was added to the water layer to basify the solution, and the solid was precipitated. The mixture was extracted with dichloromethane four times and the combined organic layer was dried over $Na_2SO_4$, filtered, and concentrated under reduced pressure. The crude product was purified by chromatography on silica gel (hexane : ethyl acetate = 2 : 1) to afford a pale green solid (0.58 g, 75% yield). It should be noted that gaseous dimethylamine is generated during the reaction and the result of this reaction is susceptible to variation, depending on the used apparatus and reaction scale. The use of a Schlenk tube rather than a round-bottomed flask with a reflux condenser is therefore recommended. Moreover, monitoring the reaction by TLC in the middle of the reaction should be avoided because dimethylamine may escape from the reaction vessel when the flask is opened.

***Synthesis of ethers*** Substrates **1a, 1c-f, 1h,** and **1s** are commercially available. Other ethers were synthesized according to the literature.[25] Descriptions of the general procedures ensue.

*General procedure A.* Benzyl bromide (1.5 equiv) was slowly added to a solution of phenol derivative

(3.0–7.5 mmol, 1.0 equiv) and $K_2CO_3$ (3.0 equiv) in DMF or $CH_3CN$ (0.38 M) at room temperature. After the addition was completed, the mixture was stirred at the indicated temperature and subsequently cooled to room temperature. Next, water was added and the mixture was extracted three times with ethyl acetate. The combined organic layer was washed with brine, dried over $Na_2SO_4$, filtered, and concentrated under reduced pressure. The crude product was purified by chromatography on silica gel or recrystallization with a mixed hexane/ethyl acetate solvent to produce the corresponding benzyl ethers.

*General procedure B*. $K_2CO_3$ (2.0 equiv) was added to a solution of phenol derivative (6.0–13.1 mmol, 1.0 equiv) and 4-methoxybenzyl chloride (1.3 equiv) in DMF (1.0 M) at room temperature. After the addition was completed, the mixture was stirred at room temperature for the period indicated below. The mixture was then poured into ice-cooled water and subsequently warmed to room temperature. The formed solid was filtered and dissolved in ethyl acetate or dichloromethane. The solution was dried over $Na_2SO_4$, filtered, and concentrated under reduced pressure. The crude product was purified by recrystallization with ethanol or a mixed hexane/ethyl acetate solvent to produce the corresponding *p*-methoxybenzyl ethers.

***4-Benzyloxybenzonitrile (1b)***[26] According to general procedure A, the title compound was prepared in DMF at 60 °C for 1 h. The crude product was purified by chromatography on silica gel (hexane : ethyl acetate = 10 : 1) to afford a white solid (1.44 g, 93%).

***4-Benzyloxy-1,1'-biphenyl (1g)***[27] According to general procedure A, the title compound was prepared in $CH_3CN$ at room temperature for 21 h. The crude product was purified by recrystallization with hexane and ethyl acetate to afford a white solid (1.28 g, 82%).

***1-Benzyloxynaphthalene (1i)***[25a] According to general procedure A, the title compound was prepared in $CH_3CN$ at 85 °C for 1 h. The crude product was purified by chromatography on silica gel (hexane : ethyl acetate = 100 : 1) to afford a white solid (0.20 g, 29%).

***2-Benzyloxynaphthalene (1j)***[28] According to general procedure A, the title compound was prepared in $CH_3CN$ at 85 °C for 1 h. The crude product was purified by recrystallization with hexane and ethyl acetate to afford a white solid (0.31 g, 44%).

***1-Methoxy-4-(phenoxymethyl)benzene (1k)***[29] According to general procedure B, the title compound was prepared for 18 h. The crude product was purified by recrystallization with ethanol to afford a white solid (1.79 g, 79%).

***4-(4-Methoxybenzyloxy)benzonitrile (1l)***[26] According to general procedure B, the title compound was prepared for 19 h. The crude product was purified by recrystallization with hexane and ethyl acetate to afford a white solid (0.99 g, 69%).

***Methyl 4-(4-methoxybenzyloxy)benzoate (1m)***[25b] According to general procedure B, the title compound was prepared for 17 h. The crude product was purified by recrystallization with ethanol to afford a white solid (3.08 g, 86%).

***1-(4-Methoxybenzyloxy)naphthalene (1n)***[25a] According to general procedure B, the title compound was prepared for 7 h. The crude product was purified by recrystallization with hexane and ethyl acetate to afford a pale orange solid (0.67 g, 42%).

***2-(4-Methoxybenzyloxy)naphthalene (1o)***[30] According to general procedure B, the title compound was prepared according to general procedure B for 7 h. The crude product was purified by recrystallization with hexane and ethyl acetate to afford a white solid (1.11 g, 70%).

***Benzyl pentyl ether (1p)***[31] Pentan-1-ol (2.4 mL, 22.6 mmol, 1.1 equiv) was added to a suspension of NaH (dry, 984 mg, 41 mmol, 2 equiv) in THF (41 mL) at 0 °C. After $H_2$ gas evolution ceased (2 h), benzyl bromide (2.5 mL, 20.5 mmol, 1 equiv) was added dropwise at 0 °C. The reaction mixture was then stirred for 18 h at 26 °C. The reaction was quenched with water, and the mixture was extracted with $Et_2O$ three times. Next, the solution was dried over $MgSO_4$, filtered, and concentrated under reduced pressure. The crude product was purified by chromatography on silica gel [hexane to hexane/ethyl acetate (50/1)] to afford **1p** (3.41 g, 84%).

***4-Dodecyloxybenzonitrile (1q)***[32] $K_2CO_3$ (4.64 g, 33.6 mmol, 5.6 equiv) was added to a solution of 4-cyanophenol (0.71 g, 6.0 mmol, 1.0 equiv) and dodecyl bromide (1.73 mL, 7.2 mmol, 1.2 equiv) in acetone (40 mL, 0.15 M) at room temperature, under air. The mixture was stirred at 60 ℃ for 17 h. After the reaction was completed, the mixture was cooled to room temperature and poured into ice-cooled water. The solid was then filtered and dissolved in ethyl acetate. Next, the solution was dried over $Na_2SO_4$, filtered, and concentrated under reduced pressure. Finally, the crude product was purified by chromatography on silica gel (hexane to ethyl acetate) to afford a white solid (1.30 g, 75%).

***4-Isopropyloxybenzonitrile (1r)***[33] $K_2CO_3$ (4.64 g, 33.6 mmol, 5.6 equiv) was added to a solution of 4-cyanophenol (0.71 g, 6.0 mmol, 1.0 equiv) and 2-iodopropane (0.72 mL, 7.2 mmol, 1.2 equiv) in acetone (40 mL, 0.15 M) at room temperature, under air. The mixture was then stirred at 60 ℃. After 73 h, another 2-iodopropane (0.36 mL, 3.6 mmol, 0.6 equiv) was added, and the mixture was stirred for a further 6 h. After the mixture was cooled to room temperature, it was concentrated under reduced pressure. Ethyl acetate was then added, and the mixture was washed twice with water and once with brine. The organic layer was dried over $Na_2SO_4$, filtered, and concentrated under reduced pressure. The crude product was purified by chromatography on silica gel (hexane : ethyl acetate = 10 : 1) to afford a colorless oil (0.94 g, 97%).

***Optimization of the photochemical C–O bond cleavage of 1a (Table 1)*** General procedure: **1a** (0.50 mmol, 1.0 equiv), photocatalyst (5 mol%), 1,4-cyclohexadiene (2 equiv), and the solvent (5.0 mL, 0.1 M) were added into a Pyrex glassware vessel. The mixture was deaerated by bubbling argon for 10 min, after which the base (2 equiv) was added. The mixture was then irradiated with a 400 nm LED lamp at 23 ℃ for 24 h or 48 h, except in entry 19 where the reaction was stirred in the dark. The yield was determined by $^1$H NMR or RP-HPLC analysis using 1,3,5-trimethoxybenzene and anisole as internal standards, respectively.

***Photochemical C–O bond cleavage of ethers (Table 2)*** General procedure: Substrate ether (0.50 mmol, 1.0 equiv), **PC3** (6.3 mg, 0.025 mmol, 5 mol%), 1,4-cyclohexadiene (93.5 μL, 1.0 mmol, 2.0 equiv), and DMSO (5.0 mL, 0.1 M) were added into a Pyrex glassware vessel. The mixture was deaerated by bubbling argon for 10 min, after which $Cs_2CO_3$ (325.8 mg, 1.0 mmol, 2.0 equiv) was added. Subsequently, the mixture was irradiated with a 400 nm LED at 23 ℃ for the indicated time (see main Table 2). Next, 1 M HCl aq. was added to the reaction mixture to adjust the pH to 3 and the resultant mixture was extracted with ethyl acetate three times. The combined organic layer was washed once with brine, dried over $Na_2SO_4$, and filtered. The filtrate was then concentrated under reduced pressure. For the non-volatile compounds, the residue was purified by chromatography on $SiO_2$ to afford the corresponding alcohols. For the volatile compounds, the indicated internal standard was added to the residue and the mixture was analyzed by $^1H$ or $^{19}F$ NMR or by RP-HPLC to determine the yield. All the products in this study (**2a**–**k**) are characterized by comparison with commercially available authentic samples.

***Entry 1, Table 2*** According to the general procedure, 4-cyanophenol (**2b**) was obtained (59 mg, 99 % yield, brown solid).

***Entry 1, Table 2* (2 mmol scale)** Substrate **1b** (0.42 g, 2.0 mmol, 1.0 equiv), **PC3** (25 mg, 0.10 mmol, 5 mol%), 1,4-cyclohexadiene (374 μL, 4.0 mmol, 2.0 equiv), and DMSO (20 mL, 0.1 M) were added into a Pyrex glassware vessel. The mixture was deaerated by bubbling argon for 10 min, after which $Cs_2CO_3$ (1.30 g, 4.0 mmol, 2.0 equiv) was added. Subsequently, the mixture was irradiated with a 400 nm LED at 23 ℃ for 29 h. Next, 1 M HCl aq. was added to the reaction mixture to adjust the pH to 3 and the resultant mixture was extracted with ethyl acetate three times. The combined organic layer was washed once with brine, dried over $Na_2SO_4$, and filtered. The filtrate was then concentrated under reduced pressure. The residue was purified by chromatography on $SiO_2$ to afford **2b** (0.23 g, 98%, brown solid).

***Entry 2, Table 2*** According to the general procedure, methyl 4-hydroxybenzoate (**2c**) was obtained (77 mg, >99% yield, yellow solid).

***Entry 3, Table 2*** According to the general procedure, 4-hydroxybenzaldehyde (**2d**) was obtained (69% yield). The yield was determined by $^1H$ NMR analysis using 1,3,5-trimethoxybenzene as the internal standard.

***Entry 4, Table 2*** According to the general procedure, 4-fluorophenol (**2e**) was obtained (68% yield). The yield was determined by $^{19}F$ NMR analysis using fluorobenzene as the internal standard.

***Entry 5, Table 2*** According to the general procedure, 4-acetylphenol (**2f**) was obtained (29 mg, 43 % yield, pale orange solid).

***Entry 6, Table 2*** According to the general procedure, 4-hydroxybiphenyl (**2g**) was obtained (60 mg, 70 % yield, white solid). $^1H$ NMR (400 MHz, $CD_3OD$): $\delta$ = 7.52 (m, 2H), 7.43 (dt, $J$ = 9.2 Hz, 2.6 Hz, 2H), 7.37 (tt, $J$ = 7.8 Hz, 1.8 Hz, 2H), 7.24 (tt, 7.2 Hz, 1.6 Hz, 1H), 6.34 (dt, 9.2 Hz, 2.4 Hz,

2H) ppm; $^{13}C\{^{1}H\}$ NMR (100 MHz, $CD_3OD$): δ = 158.2, 142.4, 133.8, 129.7, 129.0, 127.4, 127.4, 116.6 ppm.

***Entry 7, Table 2*** According to the general procedure, 4-methoxyphenol (**2h**) was obtained (25 mg, 40% yield, yellow solid).

***Entry 8, Table 2*** According to the general procedure, 1-naphthol (**2i**) was obtained (55% yield). The yield was determined by $^{1}H$ NMR analysis using 1,3,5-trimethoxybenzene as the internal standard.

***Entry 9, Table 2*** According to the general procedure, 2-naphthol (**2j**) was obtained (45 mg, 62% yield, brown solid).

***Entry 10, Table 2*** According to the general procedure, phenol (**2a**) was obtained (51% yield). The yield was determined by RP-HPLC analysis using anisole as the internal standard.

***Entry 11, Table 2*** According to the general procedure, 4-cyanophenol (**2b**) was obtained (56 mg, 93% yield, pale yellow solid).

***Entry 12, Table 2*** According to the general procedure, methyl 4-hydroxybenzoate (**2c**) was obtained (60 mg, 78% yield, pale yellow solid).

***Entry 13, Table 2*** According to the general procedure, 1-naphthol (**2i**) was obtained (35 mg, 48% yield, brown solid).

***Entry 14, Table 2.*** According to the general procedure, 2-naphthol (**2j**) was obtained (31 mg, 43% yield, orange solid).

***Entry 15, Table 2*** According to the general procedure, pentan-1-ol (**2k**) was obtained (15% yield). The yield was determined by $^{1}H$ NMR analysis using 1,3,5-trimethoxybenzene as the internal standard.

***Entry 16, Table 2.*** According to the general procedure, 4-cyanophenol (**2b**) was obtained (>99 % yield). The yield was determined by $^{1}H$ NMR analysis using 1,3,5-trimethoxybenzene as the internal standard.

***Entry 17, Table 2*** According to the general procedure, 4-cyanophenol (**2b**) was obtained (54 mg, 90% yield, pale brown solid).

***Entry 18, Table 2*** According to the general procedure, 4-cyanophenol (**2b**) was obtained (56 mg, 94% yield, brown solid).

***Study of the effects of $Cs_2CO_3$ (Figure 3).*** The DMSO in the ensuing experiments was deaerated by bubbling argon and employed in a glove box.

***Changes in the UV-vis absorption of PC3 (Figure 3a).*** A 0.1 mM solution of **PC3** in DMSO was prepared and transferred to a quartz cuvette. The cuvette was removed from the glove box and subjected to UV-vis absorption analysis. For the sample with $Cs_2CO_3$, $Cs_2CO_3$ (200 mg) was added to 3 mL of 0.1 mM DMSO solution of **PC3** in a quartz cuvette in a glove box. The suspension was then shaken and removed from the glove box. Five minutes after shaking, the insoluble $Cs_2CO_3$ residue settled at the bottom of the cuvette, after which the sample was subjected to UV-vis absorption analysis.

***Changes in the UV-vis absorption of PC1 (Figure 3b).*** A 0.1 mM solution of **PC1** in DMSO was

prepared and transferred to a quartz cuvette in a glove box. The cuvette was removed from the glove box and subjected to UV-vis absorption analysis. For the sample with $Cs_2CO_3$, $Cs_2CO_3$ (200 mg) was added to 3 mL of 0.1 mM DMSO solution of **PC1** in a quartz cuvette in a glove box, after which the suspension was shaken and removed from the glove box. Five minutes after shaking, the insoluble $Cs_2CO_3$ residue settled at the bottom of the cuvette and the sample was subjected to UV-vis absorption analysis.

***Changes in the $^1$H NMR spectra of PC3 (Figure 3c)*** A 5 mM solution of **PC3** in DMSO was prepared and transferred to an NMR tube in a glove box. The tube was removed from the glove box and subjected to $^1$H NMR analysis. For the sample with $Cs_2CO_3$, $Cs_2CO_3$ (200 mg) was added to 2.5 mL of 5 mM DMSO solution of **PC3** in a screw vial in a glove box. The mixture was shaken, and 0.7 mL of the resultant suspension was transferred to an NMR tube. The tube was removed from the glove box and left to stand until the insoluble $Cs_2CO_3$ residue settled at the bottom of the NMR tube. The sample was then subjected to $^1$H NMR analysis.

***Changes in the fluorescence spectra of PC3 (Figure 3d).*** In a glove box, $Cs_2CO_3$ (200 mg) was added to 3 mL of 5 μM DMSO solution of **PC3** in a quartz cuvette. The suspension was shaken and removed from the glove box. Five minutes after shaking, the insoluble $Cs_2CO_3$ residue settled at the bottom of the cuvette and the sample was subjected to fluorescence measurement analysis (Ex.: 365 nm). The measurements were conducted at the intervals indicated in Figure 3d.

***Reversibility of the interaction between PC3 and $Cs_2CO_3$ (Figure 3e).*** In a glove box, $Cs_2CO_3$ (200 mg) was added to 3 mL of 5 μM DMSO solution of **PC3** in a quartz cuvette. The suspension was shaken and removed from the glove box. Fifty minutes after shaking, the sample was subjected to fluorescence measurement analysis. Next, the sample was shaken and left to stand until the insoluble $Cs_2CO_3$ residue settled at the bottom of the cuvette. The sample was then subjected to fluorescence measurement analysis (Ex.: 365 nm).

***Excitation spectra of PC3 in the presence of $Cs_2CO_3$ (Figure 3f).*** In a glove box, $Cs_2CO_3$ (200 mg) was added to 3 mL of 5 μM DMSO solution of **PC3** in a quartz cuvette. The suspension was shaken and removed from the glove box. Five minutes after shaking, the insoluble $Cs_2CO_3$ residue settled at the bottom of the cuvette. The excitation spectra were measured by monitoring the fluorescence at 450 and 560 nm.

***Fluorescence quenching experiments of PC3 with quencher candidates (1a or CHD; Figure 3g).*** DMSO solutions of a mixture of **PC3** (5 μM) and the indicated concentration of **1a** or CHD were prepared in a glove box, and 3 mL of each solution was transferred to separate quartz cuvettes. For the samples with $Cs_2CO_3$, in a glove box $Cs_2CO_3$ (200 mg) was added to 3 mL of the solution prepared as mentioned above in a quartz cuvette. The samples were then removed from the glove box. The samples were excited at 365 nm and the fluorescence intensity at 447 nm was plotted, except for the samples containing **PC3**, CHD, and $Cs_2CO_3$ (green line in Figure 3g), where the fluorescence intensity at 490

nm (isofluorescent point) was plotted because the red-shifted species persisted during measurement.

***Changes in the UV-vis absorption of 1a (Figure 3h)*** A 0.1 M solution of **1a** in DMSO was prepared and transferred to a quartz cuvette in a glove box. The cuvette was removed from the glove box and subjected to UV-vis absorption analysis. For the sample with $Cs_2CO_3$, $Cs_2CO_3$ (200 mg) was added to 5 mL of a 0.1 M DMSO solution of **1a** in a quartz cuvette in a glove box. The suspension was shaken and left to stand until the insoluble $Cs_2CO_3$ residue settled at the bottom of the cuvette. The cuvette was removed from the glove box, and subjected to UV-vis absorption analysis.

## AUTHOR INFORMATION


### Corresponding Author

* matsubara.ryosuke@people.kobe-u.ac.jp


### Associated Content

### Supporting Information

CV of **1a**, absorption spectrum of **1a** in the presence of $Cs_2CO_3$, emission spectrum of the LED lamp, photoirradiation system, CV of **PC3**, discussion about the effects of $Cs_2CO_3$, absorption of dimsyl anion, quantum yield determination, $^{1}H$, $^{13}C$, $^{19}F$ NMR spectra, and RP-HPLC analysis.

### Notes

The authors declare no conflict of interest.

### Acknowledgments


This work was carried out by the joint research program of the Molecular Photoscience Research Center, Kobe University (H29001). Financial support from the Shorai Foundation for Science and Technology is greatly appreciated. This work was also supported by the Ministry of Education, Culture, Sports, Science and Technology (MEXT), Japan.


### References


(1) Zakzeski, J.; Bruijnincx, P. C.; Jongerius, A. L.; Weckhuysen, B. M., The catalytic valorization of lignin for the production of renewable chemicals. *Chem. Rev.* **2010,** *110*, 3552-3599.

(2) (a) Narayanam, J. M.; Stephenson, C. R., Visible light photoredox catalysis: applications in organic synthesis. *Chem. Soc. Rev.* **2011,** *40*, 102-113; (b) Xuan, J.; Xiao, W. J., Visible-light photoredox catalysis. *Angew. Chem. Int. Ed. Engl.* **2012,** *51*, 6828-6838; (c) Prier, C. K.; Rankic, D. A.; MacMillan, D. W., Visible light photoredox catalysis with transition metal complexes:

applications in organic synthesis. *Chem. Rev.* **2013,** *113*, 5322-5363; (d) Romero, N. A.; Nicewicz, D. A., Organic Photoredox Catalysis. *Chem. Rev.* **2016,** *116*, 10075-10166.
(3) Blanksby, S. J.; Ellison, G. B., Bond dissociation energies of organic molecules. *Acc. Chem. Res.* **2003,** *36*, 255-263.
(4) Hasegawa, E.; Takizawa, S.; Seida, T.; Yamaguchi, A.; Yamaguchi, N.; Chiba, N.; Takahashi, T.; Ikeda, H.; Akiyama, K., Photoinduced electron-transfer systems consisting of electron-donating pyrenes or anthracenes and benzimidazolines for reductive transformation of carbonyl compounds. *Tetrahedron* **2006,** *62*, 6581-6588.
(5) Larraufie, M. H.; Pellet, R.; Fensterbank, L.; Goddard, J. P.; Lacote, E.; Malacria, M.; Ollivier, C., Visible-light-induced photoreductive generation of radicals from epoxides and aziridines. *Angew. Chem. Int. Ed. Engl.* **2011,** *50*, 4463-4466.
(6) Todorov, A. R.; Wirtanen, T.; Helaja, J., Photoreductive Removal of *O*-Benzyl Groups from Oxyarene *N*-Heterocycles Assisted by *O*-Pyridine-pyridone Tautomerism. *J. Org. Chem.* **2017,** *82*, 13756-13767.
(7) (a) Nguyen, J. D.; Matsuura, B. S.; Stephenson, C. R., A photochemical strategy for lignin degradation at room temperature. *J. Am. Chem. Soc.* **2014,** *136*, 1218-1221; (b) Magallanes, G.; Kärkäs, M. D.; Bosque, I.; Lee, S.; Maldonado, S.; Stephenson, C. R. J., Selective C–O Bond Cleavage of Lignin Systems and Polymers Enabled by Sequential Palladium-Catalyzed Aerobic Oxidation and Visible-Light Photoredox Catalysis. *ACS Catalysis* **2019,** *9*, 2252-2260.
(8) Yang, C.; Kärkäs, M. D.; Magallanes, G.; Chan, K.; Stephenson, C. R. J., Organocatalytic Approach to Photochemical Lignin Fragmentation. *Org. Lett.* **2020,** *22*, 8082-8085.
(9) (a) Matsubara, R.; Shin, Y.-S.; Shimada, T.; Hayashi, M., Revisiting the Saito Photochemical Reduction and the Development of a One-Pot Deoxygenation of Alcohols. *Asian J. Org. Chem.* **2014,** *3*, 1054-1057; (b) Matsubara, R.; Shimada, T.; Kobori, Y.; Yabuta, T.; Osakai, T.; Hayashi, M., Photoinduced Charge-Transfer State of 4-Carbazolyl-3-(trifluoromethyl)benzoic Acid: Photophysical Property and Application to Reduction of Carbon-Halogen Bonds as a Sensitizer. *Chem. Asian J.* **2016,** *11*, 2006-2010.
(10) Matsubara, R.; Yabuta, T.; Idros, U. M.; Hayashi, M.; Ema, F.; Kobori, Y.; Sakata, K., UVA- and Visible-Light-Mediated Generation of Carbon Radicals from Organochlorides Using Nonmetal Photocatalyst. *J. Org. Chem.* **2018,** *83*, 9381-9390.
(11) (a) Ghosh, I.; Shaikh, R. S.; Konig, B., Sensitization-Initiated Electron Transfer for Photoredox Catalysis. *Angew. Chem. Int. Ed. Engl.* **2017,** *56*, 8544-8549; (b) Discekici, E. H.; Treat, N. J.; Poelma, S. O.; Mattson, K. M.; Hudson, Z. M.; Luo, Y.; Hawker, C. J.; Read de Alaniz, J., A highly reducing metal-free photoredox catalyst: design and application in radical dehalogenations. *Chem. Commun.* **2015,** *51*, 11705-11708.
(12) (a) Zeman, C. J. t.; Kim, S.; Zhang, F.; Schanze, K. S., Direct Observation of the Reduction

of Aryl Halides by a Photoexcited Perylene Diimide Radical Anion. *J. Am. Chem. Soc.* **2020,** *142*, 2204-2207; (b) MacKenzie, I. A.; Wang, L.; Onuska, N. P. R.; Williams, O. F.; Begam, K.; Moran, A. M.; Dunietz, B. D.; Nicewicz, D. A., Discovery and characterization of an acridine radical photoreductant. *Nature* **2020,** *580*, 76-80; (c) Cole, J. P.; Chen, D. F.; Kudisch, M.; Pearson, R. M.; Lim, C. H.; Miyake, G. M., Organocatalyzed Birch Reduction Driven by Visible Light. *J. Am. Chem. Soc.* **2020,** *142*, 13573-13581.

(13) Matsubara, R.; Kaiba, T.; Nakata, A.; Yabuta, T.; Hayashi, M.; Tsubaki, M.; Uchino, T.; Chatani, E., 9-Aryl-3-aminocarbazole as an Environment- and Stimuli-Sensitive Fluorogen and Applications in Lipid Droplet Imaging. *J. Org. Chem.* **2019,** *84*, 5535-5547.

(14) (a) Liang, K.; Liu, Q.; Shen, L.; Li, X.; Wei, D.; Zheng, L.; Xia, C., Intermolecular oxyarylation of olefins with aryl halides and TEMPOH catalyzed by the phenolate anion under visible light. *Chem. Sci.* **2020,** *11*, 6996-7002; (b) Schmalzbauer, M.; Marcon, M.; König, B., Excited State Anions in Organic Transformations. *Angew. Chem. Int. Ed.* 10.1002/anie.202009288.

(15) Rehm, D.; Weller, A., Kinetics of Fluorescence Quenching by Electron and H-Atom Transfer. *Isr. J. Chem.* **1970,** *8*, 259.

(16) Jin, S.; Dang, H. T.; Haug, G. C.; He, R.; Nguyen, V. D.; Nguyen, V. T.; Arman, H. D.; Schanze, K. S.; Larionov, O. V., Visible Light-Induced Borylation of C-O, C-N, and C-X Bonds. *J. Am. Chem. Soc.* **2020,** *142*, 1603-1613.

(17) Observed broadening of the peaks in the chart (i) is typical to 3,6-bis(dimethylamino)carbazoles and could be attributed to the restricted rotation of C–N single bonds between the carbazole and $NMe_2$ groups on the NMR time scale. The rotation restriction occurs probably due to the conjugation of the lone pair of $NMe_2$ nitrogen atoms with the carbazole pai system.

(18) Brimioulle, R.; Bach, T., Enantioselective Lewis acid catalysis of intramolecular enone [2+2] photocycloaddition reactions. *Science* **2013,** *342*, 840-843.

(19) The possibility that dimsyl anion generated from DMSO and $Cs_2CO_3$ serves as a photoexited electron donor is unlikely in this reaction, but cannot be completely ruled out. Budén, M. E.; Bardagí, J. I.; Puiatti, M.; Rossi, R. A., Initiation in Photoredox C–H Functionalization Reactions. Is Dimsyl Anion a Key Ingredient? *J. Org. Chem.* **2017,** *82*, 8325-8333. See Supporting Information for a more detailed discussion.

(20) Gentry, E. C.; Knowles, R. R., Synthetic Applications of Proton-Coupled Electron Transfer. *Acc. Chem. Res.* **2016,** *49*, 1546-1556.

(21) Tsang, W., Thermodynamic and Kinetic-Properties of the Cyclohexadienyl Radical. *J. Phys. Chem.* **1986,** *90*, 1152-1155.

(22) Bordwell, F. G.; Liu, W.-Z., Effects of sulfenyl, sulfinyl and sulfonyl groups on acidities and homolytic bond dissociation energies of adjacent C-H and N-H bonds. *J. Phys. Org. Chem.* **1998,**

*11*, 397-406.
(23) Bordwell, F. G.; Zhang, X.; Cheng, J. P., Comparisons of the acidities and homolytic bond dissociation energies of the acidic nitrogen-hydrogen and carbon-hydrogen bonds in diphenylmethanes and carbazoles. *J. Org. Chem.* **1991,** *56*, 3216-3219.
(24) (a) Elvington, M.; Brewer, K., Electrochemistry. In *Application of Physical Methods to Inorganic and Bioinorganic Chemistry*, Scott, R. A.; Lukehart, C. M., Eds. Wiley: Chichester, **2007**; pp 17-38; (b) Gennett, T.; Milner, D. F.; Weaver, M. J., Role of solvent reorganization dynamics in electron-transfer processes. Theory-experiment comparisons for electrochemical and homogeneous electron exchange involving metallocene redox couples. *J. Phys. Chem.* **1985,** *89*, 2787-2794.
(25) (a) Mao, Y.; Liu, Y.; Hu, Y.; Wang, L.; Zhang, S.; Wang, W., Pd-Catalyzed Debenzylation and Deallylation of Ethers and Esters with Sodium Hydride. *ACS Catalysis* **2018,** *8*, 3016-3020; (b) Swanger, S. A.; Vance, K. M.; Acker, T. M.; Zimmerman, S. S.; DiRaddo, J. O.; Myers, S. J.; Bundgaard, C.; Mosley, C. A.; Summer, S. L.; Menaldino, D. S.; Jensen, H. S.; Liotta, D. C.; Traynelis, S. F., A Novel Negative Allosteric Modulator Selective for GluN2C/2D-Containing NMDA Receptors Inhibits Synaptic Transmission in Hippocampal Interneurons. *ACS Chem. Neurosci.* **2018,** *9*, 306-319.
(26) Shigeno, M.; Hayashi, K.; Nozawa-Kumada, K.; Kondo, Y., Phosphazene Base tBu-P4 Catalyzed Methoxy–Alkoxy Exchange Reaction on (Hetero)Arenes. *Chem. Eur. J.* **2019,** *25*, 6077-6081.
(27) Percec, V.; Golding, G. M.; Smidrkal, J.; Weichold, O., $NiCl_2$(dppe)-Catalyzed Cross-Coupling of Aryl Mesylates, Arenesulfonates, and Halides with Arylboronic Acids. *J. Org. Chem.* **2004,** *69*, 3447-3452.
(28) Li, G.; Nieves-Quinones, Y.; Zhang, H.; Liang, Q.; Su, S.; Liu, Q.; Kozlowski, M. C.; Jia, T., Transition-metal-free formal cross-coupling of aryl methyl sulfoxides and alcohols via nucleophilic activation of C-S bond. *Nat. Commun.* **2020,** *11*, 2890.
(29) Kuwano, R.; Kusano, H., Benzyl Protection of Phenols under Neutral Conditions: Palladium-Catalyzed Benzylations of Phenols. *Org. Lett.* **2008,** *10*, 1979-1982.
(30) Escobar, R. A.; Johannes, J. W., A Unified and Practical Method for Carbon–Heteroatom Cross-Coupling using Nickel/Photo Dual Catalysis. *Chem. Eur. J.* **2020,** *26*, 5168-5173.
(31) Urgoitia, G.; SanMartin, R.; Herrero, M. T.; Domínguez, E., Vanadium-Catalyzed Oxidative Debenzylation of O-Benzyl Ethers at ppm Level. *Adv. Synth. Catal.* **2016,** *358*, 3307-3312.
(32) Seo, M.; Kim, J. H.; Seo, G.; Shin, C.-H.; Kim, S. Y., Utilization of Evaporation during the Crystallization Process: Self-Templation of Organic Parallelogrammatic Pipes. *Chem. Eur. J.* **2009,** *15*, 612-622.
(33) Lee, J.; Kang, S.-U.; Lim, J.-O.; Choi, H.-K.; Jin, M.-k.; Toth, A.; Pearce, L. V.; Tran, R.;

Wang, Y.; Szabo, T.; Blumberg, P. M., N-[4-(Methylsulfonylamino)benzyl]thiourea analogues as vanilloid receptor antagonists: analysis of structure–activity relationships for the 'C-Region'. *Biorg. Med. Chem.* **2004,** *12,* 371-385.